4-5570-M-454, Aerojet-General Corp., Sacramento, Calif. (March 1964).

[9] Sabadell, A. J., Wenograd, J., and Summerfield, M., "The measurement of temperature profiles through solid propellant flames using fine thermocouples," AIAA Preprint 64-106 (January 1964); also AIAA J. (to be published).

[10] Ciepluch, C. C., "The effect of rapid pressure decay on solid propellant combustion," ARS J. **31**, 1584–1586 (1961).

[11] Mathews, S. F. and St. John, A. D., "Unsteady state solid propellant burning," Rept. RTD-TDR-63-1028, Contract AF 04(611)5171, Midwest Research Institute, Kansas City, Mo. (April 1963).

[12] Paul, B. E., Lovine, R. L., and Fong, L. Y., "A ballistic explanation of the ignition pressure peak," AIAA Preprint 64-121 (January 1964).

[13] Summerfield, M., Sutherland, G. S., Webb, M. J., Taback, H. J., and Hall, K. P., "Burning mechanism of ammonium perchlorate propellants," *Progress in Astronautics and Rocketry: Solid Propellant Rocket Research*, edited by M. Summerfield (Academic Press Inc., New York, 1960), Vol. 1, pp. 141–182.

[14] Von Elbe, G., "Theory of solid propellant ignition and response to pressure transients," 19th JANAF Meeting, Vol. III, pp. 95–127 (July 1963).

[15] Bircumshaw, L. L. and Newman, B. H., "The thermal decomposition of ammonium perchlorate, Part I." Proc. Royal Soc. (London) **A227**, 115–132 (1954).

[16] Rosser, W. A. et al., "Study of the mechanisms of fire extinguishment of propellants," Aeronautical Systems Div., Rept. ASD-TR-61-143, Contract AF 33(616)6853, Stanford Research Institute, Palo Alto, Calif. (July 1961).

[17] "Survey of recent research on flame extinguishment," Aeronautical Systems Div., Rept. ASD-TR-61-408, Dir/Aeromechanics, Flight Accessories Lab., Wright-Patterson Air Force Base, Ohio (December 1962).

[18] Sibbett, D. J., private communication. Aerojet-General Corp., Azusa, Calif. (April 1963).

[19] Ryan, N. W., Mitchell, R. C., Keller, J. A., and Baer, A. D., "Ignition and combustion of solid propellants," Final TR AFQSR 2225, Contract AF 49(638)-170, University of Utah, Salt Lake City, Utah, (September 1961).

[20] Markstein, G. H., "A shock tube study of flame front-pressure wave interaction," *6th Symposium (International) on Combustion* (Reinhold Publishing Corp., New York, 1956).

MAY-JUNE 1965 J. SPACECRAFT VOL. 2, NO. 3

Ablation of Refrasil-Phenolic Nozzle Inserts in Solid Propellant Exhausts

JAMES R. WILHELM*
Douglas Aircraft Company, Inc., Santa Monica, Calif.

Two major problems encountered in the design of high-density, edge-grain inserts are 1) the prediction of ablative behavior over a broad spectrum of propellant chemistry, and 2) the correlation of results of subscale tests with ablation rates observed in full-scale motor firings. Based on conventional heat-transfer theory and an equilibrium thermochemical analysis of the decomposition process, an attempt is made to explain measured throat ablation rates in terms of the various environmental and scaling parameters. The data used comprise results of 56 full- and subscale nozzle firings and reflect a wide variety of motor operating conditions. Preliminary analysis indicates that effective surface ablation temperature, and thus heat-transfer rate, depends upon the extent of oxidation of the char residue by the external stream. This conclusion is based on the apparent increase of calculated ablation temperatures accompanying increasing diffusion of water vapor to the insert surface. A mechanism is proposed which would explain such behavior in terms of environmentally induced surface composition. Although the concept is largely speculative, further investigation of surface oxidation effects seems warranted.

Nomenclature

C_i = mass concentration of ith product, ρ_i/ρ
c = specific heat of refrasil-phenolic, Btu/lb-°F
$\bar{c}_p$ = specific heat of exhaust gas mixture, Btu/lb-°F
$\bar{c}_{p,A}$ = specific heat of refrasil-phenolic ablation products, Btu/lb-°F
D_i = binary diffusion coefficient of exhaust product i, ft²/sec
d_* = nozzle throat diameter, in.
f = nondimensional oxidation parameter, $h_c C_{wv,\,e}/\bar{c}_p \omega \dot{\delta}$
h_c = convective heat-transfer coefficient, Btu/ft²-sec-°F
h = enthalpy of exhaust gas mixture, Btu/lb
h_r = recovery enthalpy of exhaust gas mixture, $h + r(u_e^2/2)$, Btu/lb
H = local heat-transfer potential, $h_r - h_{r,\,s}$, Btu/lb
H_T = total heat-transfer potential, $h_{r,\,e} - h_{r,\,s}$, Btu/lb
$\bar{H}$ = nondimensional heat-transfer potential, H/H_T
k = thermal conductivity of the exhaust gas mixture, Btu/ft-sec-°F
Le_i = Lewis number of ith product, $\rho D_i \bar{c}_p/k$
$\dot{m}_i$ = mass flux of exhaust product i normal to the surface, lb/ft²-sec
$\dot{m}_c'$ = rate of oxidation of surface carbon, lb/ft²-sec
$\dot{m}_c''$ = rate of appearance of surface carbon, lb/ft²-sec
M = molecular weight
P_c = chamber pressure, psi
$\bar{P}_c$ = average chamber pressure, $(1/t_q)\int P_c dt$
Pr = Prandtl number of the exhaust gas mixture, $\bar{c}_p \mu/k$
q = heat conduction variable, $(k/\bar{c}_p)(\partial H/\partial y)$, Btu/ft²-sec
q_c = convective heat flux, $h_c H_T/\bar{c}_p$, Btu/ft²-sec
q_{c0} = convective heat flux to a nonablating surface, Btu/ft²-sec
q_r = net radiant heat flux, Btu/ft²-sec
q_t = total heat flux, $q_c + q_r$, Btu/ft²-sec
Q_A = heat of ablation = $Q_D + \int c dT$, Btu/lb
Q_D = heat of decomposition, Btu/lb
r = turbulent recovery factor

Presented as Preprint 64-223 at the 1st AIAA Annual Meeting, Washington, D. C., June 29–July 2, 1964; revision received October 13, 1964.

* Chief, Physical Chemistry Section, Advance Missile Technology. Member AIAA.

R = universal gas constant, ft-lb/lb-°R
t = time, sec
t_q = equilibrium burning time, sec
T = static temperature, °R
$T_{SiO_2}{}^R$ = temperature for complete decomposition of silica in the presence of carbon, °F
$T_{SiO_2}{}^V$ = vaporization temperature of silica, °F
u = x component of exhaust gas velocity, fps
v = y component of exhaust gas velocity, fps
x = coordinate parallel to surface, ft
X = mole fraction
y = coordinate normal to surface, ft
α = radiant absorptivity
$\dot{\delta}$ = surface regression rate (radial), fps
ϵ = radiant emissivity
μ = viscosity of exhaust gas mixture, lb/ft-sec
ρ = density of exhaust gas mixture = $\sum \rho_i$, lb/ft³
σ = Stefan-Boltzmann constant, Btu/ft²-sec-°R⁴
ω = density of refrasil-phenolic, lb/ft³

Subscripts

c = particle cloud
e = outer edge of boundary layer
0 = initial conditions
s = surface conditions
wv = water vapor

Introduction

OWING to their widespread use in propulsion systems, the ablative behavior of reinforced plastics, particularly that of refrasil-phenolic, has long been the subject of research activities at Douglas. The prediction of surface ablation rates, however, although satisfactory for most design purposes, has remained deficient in certain respects. In nozzle applications the major difficulties have been 1) to correlate ablative behavior over a wide range of propellant chemistry, and 2) to relate the results of subscale materials evaluation tests with ablation rates observed in full-scale motor firings. The study presented here was performed in the hope of resolving these problems.

Because of the effect on ballistic performance, ablation in the throat region of a rocket nozzle constitutes a particularly important design consideration. For this reason, the present investigation was confined entirely to the ablation of throat inserts. The analysis should apply, however, to the ablative behavior of refrasil-phenolic at almost any location within the motor system.

Insert Ablation Data

The data utilized in this study comprise results of 56 static firings including subscale tests as well as tests of actual, full-scale motors. In most cases, identical propellant formulations were employed in both the 13- × 20-in. subscale motors as were fired in full-scale tests. Thus, the so-called "scaling" effects could be investigated. The various propellants included polysulfide, nitrile, petrin-acrylate, and polybutadiene acrylic acid (PBAA), fuel systems utilizing ammonium perchlorate as an oxidizer. Aluminum-additive weight contents varied from 2 to 18%.

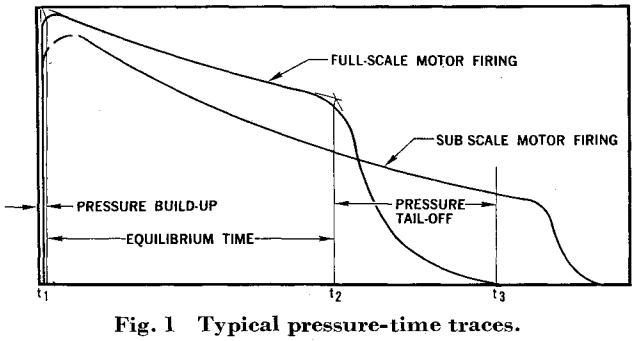

Fig. 1 Typical pressure-time traces.

All of the nozzles were of conical design with 30° and 15° entrance- and exit-cone half-angles, respectively. Initial throat diameters for the large motors varied from 10 to 11 in. as compared with diameters of approximately 1 in. in the geometrically similar, subscale nozzles. The throat inserts were constructed of high-pressure molded, edge-grain laminates containing 25 wt % phenolic resin and 75 wt % refrasil fiber. Edge-grain refrasil-phenolic, backed by phenolic-impregnated Fiberglas cloth, was employed as the entrance- and exit-cone liner material.

Initial and final throat diameters were taken as the average of three measurements made at 120° intervals around the circumference of the insert. By employing equilibrium burning times as defined in Fig. 1, average radial ablation rates during the equilibrium interval were computed. Because of the highly regressive nature of most subscale pressure histories (Fig. 1), tailoff losses can be neglected. In many full-scale firings, however, approximately 10 to 15% of the total surface ablation is estimated to have occurred during the tailoff period. The effect was more pronounced in the full-scale tests because of the high pressures at the start of tailoff (more neutral pressure profiles) and generally shorter firing durations. Correcting for tailoff losses involved a certain amount of iteration since ablation is a function of heat-flux rate, and thus surface temperature and surface temperature calculations, as will be seen later, were, in turn, based on ablation rate.

Heat-Transfer Calculations

Convective Heat Transfer

Calculations were first made to determine heating rates at the nozzle throat. Convective heat-transfer coefficients, based on Mayer's turbulent boundary-layer analysis,[1] were computed as a function of chamber pressure. For the nearly linear pressure histories observed in these firings, an effective heat-flux rate q_c based on average chamber pressure $\bar{P}_c$ yields an excellent approximation to the total convective heat input integrated over the equilibrium burning time, i.e.,

$$q_c(\bar{P}_c) = \frac{1}{t_q}\int_{t_1}^{t_2} q_c(P_c)dt \qquad (1)$$

From equilibrium thermochemical calculations, exhaust composition and molecular weights were obtained for each of the propellant formulations. Corresponding ideal-gas properties were based on an assumed specific heat ratio of 1.2. Because of uncertainties in evaluating certain heats of formation, however, total temperatures, as a function of pressure, were based on quotations by the respective propellant manufacturers. The resultant heat-flux rates were then corrected for turbulent mass-transfer effects by means of the empirical expression proposed by Arne[2]:

$$q_c/q_0 = 1 - 0.36A^{0.8}B + 0.0649A^{1.6}B^2 - 0.00778A^{2.4}B^3 + 0.00007A^{3.2}B^4 \qquad (2)$$

where

$$A = \bar{c}_{p,\,A}/\bar{c}_p \qquad B = \omega\dot{\delta}H_T/q_{c0}$$

For values of $(\omega\dot{\delta}H_T/q_{c0}) < 0.5$, the last three terms can be dropped. Assuming the specific heats of ablation and exhaust products to be approximately equal, Eq. (2) then reduces to

$$q_c/q_{c0} = 1 - 0.36\omega\dot{\delta}H_T/q_{c0} \qquad (3)$$

The convective heat-flux rates calculated from Eq. (3) are presented in Table 1.

Radiation Heat Transfer

The corresponding radiant heat-flux rates were calculated according to the analysis of Ref. 3. The incident flux from the gas-particle cloud is first determined. Since, in aluminized propellant exhausts, the radiant contribution of the gas phase is usually small compared with that of the Al_2O_3 particle cloud, gas-phase radiation has been neglected. The incident flux can therefore be written as

$$q_r' = \epsilon_c \sigma T_c^4 \quad (4)$$

where the effective emissivity of the particle cloud ϵ_c is computed as a function of local pressure and temperature, particle concentration, and nozzle geometry. Calculated emission was found to approach blackbody conditions in most of these exhaust environments. Also, with the exception of the low aluminum-content polysulfides, there was no appreciable difference in the magnitude of radiation between subscale and full-scale nozzles.

To determine the net radiant flux at the throat, the radiant interchange with adjacent nozzle surfaces (Fig. 2) must be taken into account. Employing conventional engineering analysis, the net radiant flux to the surface, considering absorption and reflection by the particle cloud, is found to be

$$q_r = (\alpha_s \epsilon_c \sigma T_c^4 - \alpha_c \epsilon_s \sigma T_s^4)/[1 - (1 - \alpha_c)(1 - \alpha_s)] \quad (5)$$

If it is further assumed that surface and cloud absorptivities are equal to their respective emissivities, Eq. (5) becomes

$$q_r = [\epsilon_c \epsilon_s \sigma (T_c^4 - T_s^4)]/[1 - (1 - \epsilon_c)(1 - \epsilon_s)] \quad (6)$$

In evaluating Eq. (6), a constant surface emissivity ϵ_s of 0.8 is assumed.

The total heat flux q_t at the surface is then taken as the sum of the net radiant heat-transfer rate and the convective heat-transfer rate corrected for mass-transfer effects, i.e.,

$$q_t = q_c + q_r \quad (7)$$

But until surface temperatures are specified, the heat-transfer rates cannot be determined. For purposes of comparison, heat-flux values given in Table 1 are based on an assumed surface temperature of 4000°F.

Table 1 Insert ablation data

Propellant and conditions	$\bar{P}_c$, psia	Heat fluxes, Btu/ft²-sec q_c	q_t	$\dot{\delta}$, mil/sec
2% Al-Polysulfide (PSA)				
$d_* = 1.0$ in.	409	248	280	2.1
$T_C = 4780$°F	481	278	310	3.2
$X_{wv} = 0.367$	498	289	321	2.9
	423	247	279	3.6
	438	258	290	3.5
	528	305	337	5.1
	506	289	321	4.8
	516	294	326	2.6
	405	242	275	3.4
	490	283	315	2.2
	434	256	288	3.5
2% Al-Polysulfide (PSB)				
$d_* = 1.0$ in.	665	434	468	3.8
$T_C = 4890$°F	690	447	481	4.3
$X_{wv} = 0.379$	675	440	474	3.9
	668	436	470	5.0
	735	470	504	4.5
	669	436	470	3.9
	680	443	477	3.8
	688	446	480	4.0
$d_* = 10.5$ in.	584	258	346	6.5
	598	264	352	7.0
	565	252	340	6.6
	567	252	340	5.9
	590	260	348	6.9
	545	245	333	5.8
12% Al-nitrile (NA)				
$d_* = 1.0$ in.	607	502	643	12.3
$T_c = 5190$°F	562	471	612	12.0
$X_{wv} = 0.140$	530	449	590	11.9
	553	464	605	13.2
	548	440	581	13.3
$d_* = 10.5$ in.	760	417	566	12.9
	815	442	591	12.4
	877	476	625	13.4
12% Al-nitrile (NB)				
$d_* = 10.5$ in.	996	548	696	17.3
$T_c = 5200$°F	925	513	661	17.4
$X_{wv} = 0.147$	950	525	673	15.7
	936	518	666	15.4
	1012	554	702	15.6
	920	510	658	14.7
	1050	575	723	16.2
16% Al- (PBAA) polybutadiene acrylic acid				
$d_* = 1.0$ in.	703	700	880	18.2
$T_c = 5290$°F	700	700	880	19.8
$X_{wv} = 0.093$	605	621	801	17.9
	709	705	885	19.7
$d_* = 10.5$ in.	905	601	785	19.6
	990	644	929	23.0
	938	618	802	19.7
	898	591	775	18.5
	743	501	685	15.6
	989	644	828	15.6
	923	606	790	20.7
	997	647	831	18.5
18% Al-Petrin (PA) acrylate				
$d_* = 1.0$ in.	446	735	1147	27.8
$T_c = 6260$°F	457	746	1158	28.4
$X_{wv} = 0.167$	452	744	1156	27.0
	461	755	1167	29.3

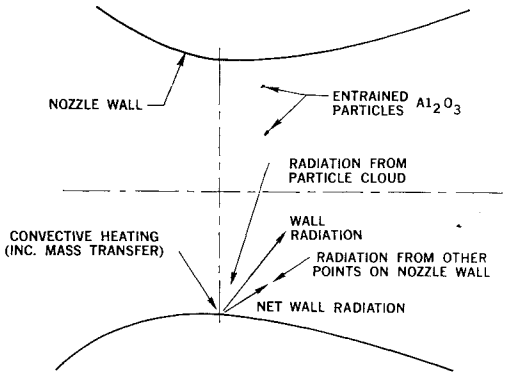

Fig. 2 Heat transfer at rocket nozzle throat.

Mechanisms of Ablation

Thermochemical Processes

The ablation model assumed in this analysis is illustrated in Fig. 3. Initially, the phenolic resin undergoes thermal breakdown or pyrolysis in the approximate temperature range of 400° to 1000°F. The pyrolysis products are then assumed to diffuse to the surface through, and in thermal equilibrium with, the resulting char layer. Subsequent reduction of the silica fiber by carbonaceous residue can then proceed according to the following heterogeneous mechanisms:

$$C + SiO_2 \rightleftarrows SiO + CO \quad (8)$$

$$2C + SiO_2 \rightleftarrows Si + 2CO \quad (9)$$

$$3C + SiO_2 \rightleftarrows SiC + 2CO \quad (10)$$

The importance of carbon-silica system chemistry in the

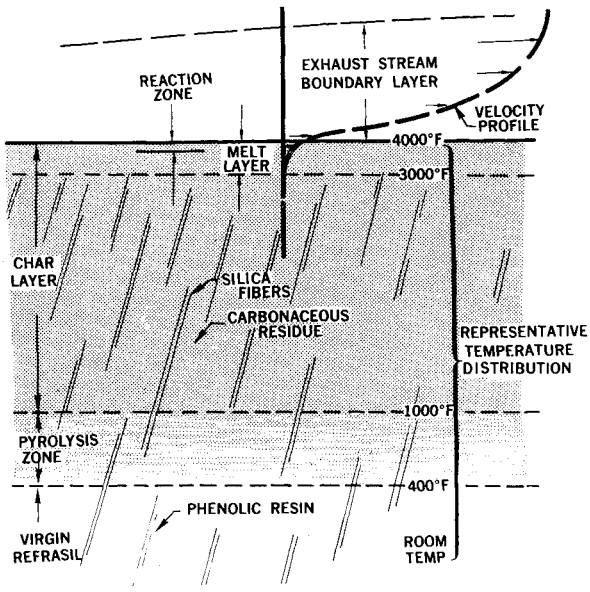

Fig. 3 Ablation schematic, phenolic-refrasil.

ablation of silica-reinforced resins is well established. Beecher and Rosensweig,[4] for example, found these reactions to proceed rapidly, even at temperatures below 3000°F. More recent experimental results[5] offer additional support to these findings. The main problem, then, is to determine which carbon-silica interactions predominate under rocket nozzle throat conditions.

At low temperatures, equilibrium calculations[5–7] show reactions (9) and (10) to be of major importance. But at temperatures above 3000°F, and at high pressures, the equilibrium mole fractions of Si and SiC become very small compared with that of SiO. Unlike the usual treatment of the carbon-silica system in ablation studies, the analysis employed here considers equilibrium conditions to be approached only within a thin reaction zone near the surface, i.e., in a region where temperatures are of the order of 3500°F and higher. With this constraint, the theoretical decomposition of the carbon-silica system proceeds primarily through the equimolar reaction of Eq. (8). The important consequence of this is that an excess of carbon is theoretically available for the reduction of silica; an excess of silica would be predicted[5–7] if equilibrium conditions were assumed to prevail throughout the char layer. As will be seen later, the analytical results are supported in part by the carbonaceous character of postfired insert surfaces and the apparent absence of subsurface SiC formation.

Thermochemical calculations were performed to examine the over-all decomposition process as a function of temperature and pressure. Within the reaction zone (Fig. 3), equilibrium was assumed to prevail between all possible decomposition products and their respective phases. Although the carbon-silica interaction in a flowing exhaust environment would by definition be a nonequilibrium process, reaction rates at the anticipated surface temperature levels may be sufficiently high so that equilibrium conditions are actually approached. Since the reaction zone is imagined to consist of small carbon particles entrained in a silica melt layer, the area available for reaction would be quite large; this would also contribute to rapid reaction rates. Initially at least, no consideration is taken of interactions with the external exhaust stream.

For the gram-atom ratios corresponding to 75% refrasil/25% phenolic resin

$$C_{7.53}H_{6.04}O_{12.24}Si_{5.62}$$

approximately 5 mole % of carbon (Fig. 4) would remain upon total reduction of the silica. Such excess carbon would then be removed by shear forces or consumed in subsequent reactions with the ablation products and/or the external gas stream.

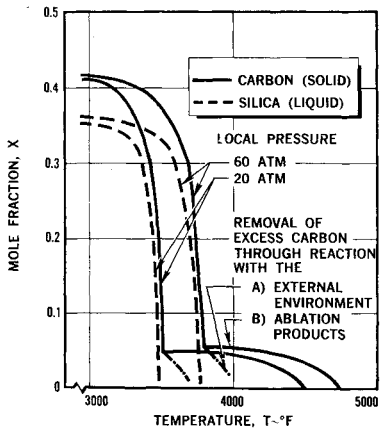

Fig. 4 Equilibrium decomposition of carbon-silica char layer refrasil-phenolic, $C_{7.53}H_{6.04}O_{12.24}Si_{5.62}$.

Abrasion and Shear Removal

Based on two-phase flow calculations employing an analysis similar to that of Ref. 8, abrasion of an insert caused by particle impact could proceed to only a minor extent. For aluminum oxide particles in the size range characteristic of solid-propellant combustion (1 to 10 μ), particle trajectories in the throat region were found to coincide almost exactly with the direction of the exhaust-gas streamlines. Thus, transport of particles to the surface would be a result of random fluctuation rather than direct impingement. Except for the possible formation of a low-viscosity alumina-silicate, the importance of alumina-surface interaction is discounted.

The magnitude of silica melt-layer shear losses was investigated over a wide range of motor operating conditions. These calculations, employing a steady-state solution[2] based on the melting ablation theory of Hidalgo,[9] indicate that the mass flow along the surface would be quite small compared with total ablation rates. Thus, carbon particles entrained in the melt layer would not be subject to an appreciable rate of flow removal. As will be pointed out in later discussion, the consumption of carbon residue appears a much more probable consequence of oxidation by the external stream. For the time being, then, the material system is assumed constrained to regress because of purely thermochemical means.

Ablation Parameters

Heat-Flux Rates

Under conditions of high heat-flux rate, the ablation of refrasil-phenolic is assumed to reach steady state almost instantly. The ablation rate $\dot{\delta}$ should, therefore, vary with total heat flux according to the steady-state energy balance

$$\dot{\delta} = q_t/\omega Q_A \qquad (11)$$

The relationship between observed ablation rates and total heat flux, assuming a fixed surface temperature of 4000°F, is shown in Fig. 5. Except for the behavior of the polysulfide (PS) data, the correlation is reasonably good. The results of the polysulfide-B (PSB) firings (Fig. 5) were particularly puzzling. Full-scale throat inserts appear to have sustained 40% higher ablation than the subscale inserts, which were exposed to less severe heat-transfer conditions. Although analysis of PSB insert surface deposits revealed incomplete combustion of aluminum, the estimated reduction in theoretical flame temperature could not begin to explain the disparity in ablation rates. Further analysis of the ablation process was therefore undertaken.

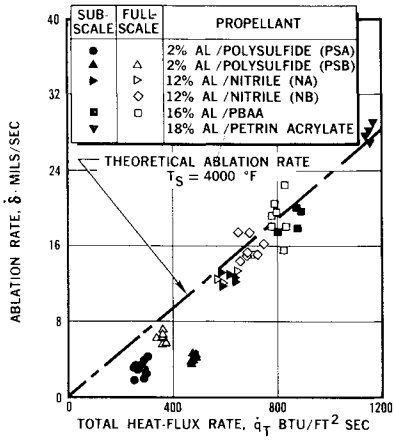

Fig. 5 Variation of ablation rate with total heat flux assuming a fixed surface temperature of 4000°F.

Heats of Ablation

The theoretical heats of ablation Q_A for refrasil-phenolic (Fig. 6) were computed according to the procedures previously outlined. These values represent the energy input required to bring the system (including all of the products and their respective phases) to thermochemical equilibrium at a given temperature level. As such, heats of ablation include both internal and sensible energy absorption, i.e.,

$$Q_A = Q_D + \int_{T_0}^{T_s} c dT \tag{12}$$

The discontinuities in the curves of Fig. 6 correspond to the disappearance of the silica, and subsequently of carbon, as illustrated in Fig. 4. Although these calculations do not consider equilibria between ablation and exhaust products, heats of ablation have been modified (as shown in Fig. 6) to account for the heat absorption associated with complete oxidation of excess carbon by water vapor.

It should be noted that for fully decomposing material, heats of ablation increase only slightly with rising surface temperature. Thus, according to Eq. (11), ablation rates should become very nearly proportional to total heat-flux rate.

Surface Ablation Temperature

Calculated surface temperature

The concept associated with the availability of excess carbon suggests two possible extremes of surface ablation temperature. In the presence of excess carbon, decomposition of the silica fiber was found from equilibrium calculations (Fig. 4) to be essentially complete at reaction temperatures

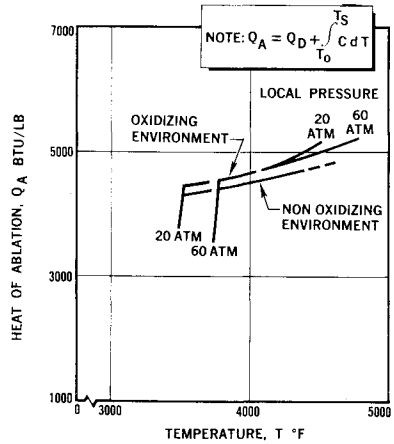

Fig. 6 Equilibrium heats of ablation of refrasil - phenolic, $C_{7.53}H_{6.04}O_{12.24}Si_{5.62}$.

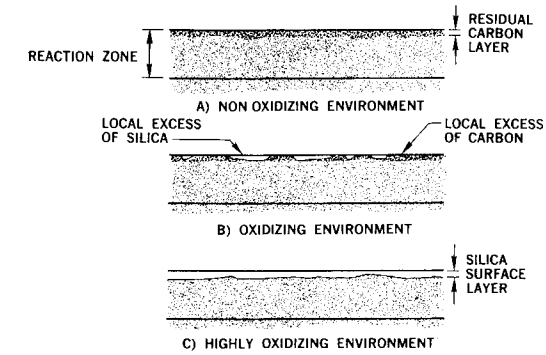

Fig. 7 Environmental effect on surface composition.

$T_{SiO_2}{}^R$ below 3800°F. Because of aerodynamic shear stresses, any residual carbon layer would be quite thin; surface temperatures, therefore, would also be of the order of 3800°F or less. Conversely, if the environment were sufficiently reactive, diffusion of oxidizing species to the surface could result in sufficient consumption of carbon to produce a surface layer composed largely of silica. In this event, surface temperatures would tend to approach the vaporization temperature of silica $T_{SiO_2}{}^V$, which, for the conditions considered here, would approach boundary-layer recovery temperatures. The transition of surface structure between these extremes is illustrated schematically in Fig. 7.

To explore the relationship between surface behavior and environmental conditions (assuming one exists), ablation temperatures were calculated for each motor firing. As shown in Fig. 8, these values were obtained by plotting heats of ablation Q_A from Eq. (11) and from equilibrium calculations as a function of temperature. Apparent surface temperatures were then found from the intersection of the two curves. As should be evident from Fig. 5, temperatures calculated in this manner from the polysulfide-A (PSA) and PSB motor firing data were significantly higher than those corresponding to the more highly aluminized fuel systems.

Surface oxidation analysis

Parallel studies in the field of graphite oxidation[10] show water vapor to be the principal oxidizing constituent in solid-propellant exhaust gas systems. To investigate possible oxidation effects, the equations expressing the transport of water vapor were therefore developed.

Assuming Fick's law is valid for a multicomponent mixture, the molecular rate of diffusion of water vapor through the boundary layer may be expressed as

$$\dot{m}_{wv} = -\rho D_{wv}(\partial C_{wv}/\partial y) \tag{13}$$

Since thermal and pressure-gradient diffusion effects have been neglected, Eq. (13) is assumed to represent the total

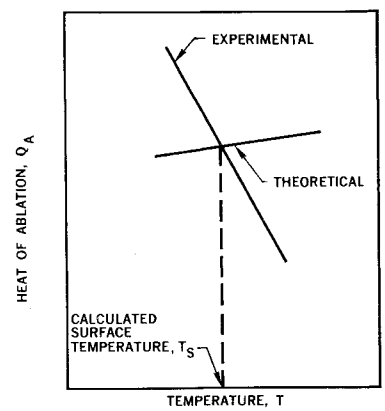

Fig. 8 Surface temperature determination.

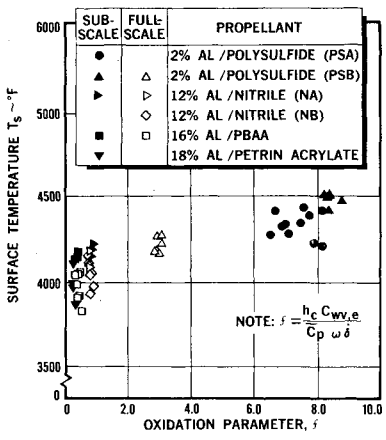

Fig. 9 Surface temperature correlation.

diffusion of water vapor in the laminar region near the surface.

Introducing the heat conduction term

$$q = (k/\bar{c}_p)(\partial H/\partial y) \tag{14}$$

and noting from Reynolds' analogy that $C = C(H)$, Eq. (13) may be rewritten as

$$\dot{m}_{wv} = -(\rho D_{wv}\bar{c}_p/k)(q/H_T)(dC_{wv}/d\bar{H}) \tag{15}$$

As in laminar boundary-layer analysis, the Prandtl and Lewis numbers are taken equal to one ($Pr = Le_i = 1$), and all of the exhaust species are assumed to have equal gas-phase diffusion coefficients. Then, from Eq. (15)

$$\dot{m}_{wv} = -(q/H_T)(dC_{wv}/d\bar{H}) \tag{16}$$

Under these conditions it also follows that stagnation enthalpy and species concentrations are linearly related throughout the boundary layer. Since the nonradiative heat transfer at the surface q_s is predominantly caused by conduction through the laminar sublayer

$$q_s = (k/\bar{c}_p)(\partial H/\partial y)_s = h_c H_T/\bar{c}_p \tag{17}$$

the rate of transport of water vapor to the surface is finally written as

$$\dot{m}_{wv,\,s} = (h_c/\bar{c}_p)(dC_{wv}/d\bar{H}) = (h_c/\bar{c}_p)C_{wv} \tag{18}$$

where

$$C_{wv} = C_{wv,\,e} - C_{wv,\,s} \tag{19}$$

In Eq. (18), the convective heat-transfer coefficient h_c has been modified through Eq. (2) to account for mass-transfer effects.

Assuming the rate of oxidation of carbon $\dot{m}_c'$ to be essentially diffusion-controlled at surface temperature levels, it follows from Eq. (18) that

$$\dot{m}_c' = M_c h_c C_{wv,\,e}\theta/M_{wv}\,\bar{c}_p \tag{20}$$

where the factor θ represents the fraction of surface area covered by carbon. It should be noted that Eq. (20) is simply an application of the well-known Lewis relation of elementary mass-transfer theory.[11]

Consistent with the preceding equilibrium analysis, the internal carbon-silica reaction is assumed to proceed at an infinite rate. The rate of appearance of carbon at the surface $\dot{m}_c'$ would, therefore, be proportional to the surface ablation rate, i.e.,

$$\dot{m}_c'' = \text{const}_1(\omega\dot{\delta}) \tag{21}$$

which is, in turn, a function of local heat-transfer conditions.

If the rate of appearance of carbon exceeds the rate at which it can be oxidized, a residue would tend to develop at the surface, its thickness limited by the combined effects of oxidation and shear removal. In the environments considered here, however, such an accumulation of surface carbon seems unlikely in light of the high rates of oxidation of graphite under similar conditions. High-density, graphite blast-tube liners,[10] for example, eroded from 3.5 to 4.0 mil/sec in 17% Al/PBAA exhaust exposure. Although the refrasil inserts regressed at four times this rate, the mass fraction of carbon involved would have been considerably less than 0.14 lb/lb material ablated. In more oxidizing exhaust systems the probability of a build-up of surface carbon is even less. Shearing effects have, therefore, been neglected, and the rate of oxidation of carbon is assumed equal to its rate of appearance. Thus, from Eqs. (20) and (21)

$$\theta f = \text{const}_2 \tag{22}$$

where

$$f = h_c C_{wv,\,e}/\bar{c}_p\omega\dot{\delta} \tag{23}$$

Assuming that the ablating surface consists of alternate regions of excess carbon and excess silica, the effective surface temperature T_S is simply the weighted average of the local temperatures corresponding to these extremes of surface composition, i.e.,

$$T_S = \theta T_{SiO_2{}^R} + (1 - \theta)T_{SiO_2{}^V} \tag{24}$$

Solving Eq. (24), the fractional area of the surface covered by carbon θ is found numerically equal to the temperature ratio

$$\theta = (T_{SiO_2{}^V} - T_S)/(T_{SiO_2{}^V} - T_{SiO_2{}^R}) \tag{25}$$

Since reaction temperatures $T_{SiO_2{}^V}$ and $T_{SiO_2{}^R}$ are relatively insensitive to pressure, the surface ablation temperature T_s becomes, according to Eq. (22), a linear function of the nondimensional oxidation parameter f.

Environmental correlation

An attempt was made to correlate surface ablation temperature in terms of the oxidation parameter f. Since calculated surface temperatures are also based on ablation rates, an artificial sensitivity would emerge between these temperatures and the corresponding parameters. To alleviate this effect, oxidation parameters have been evaluated in terms of the average ablation rate for each group of motor firings. Also, since the data from the highly aluminized propellant firings are clustered over a narrow range of oxidation potential, a logarithmic presentation has been included. Variations in calculated temperature, obscured in the display of Fig. 9, become apparent in Fig. 10.

As seen in Fig. 9, surface temperatures appear to increase more or less linearly with the nondimensional parameter f. This increase suggests the gradual development of a continuous silica melt layer as the exhaust products become progressively more oxidizing. Of particular interest are the PSB data points. The apparent disparity in ablative behavior between full- and subscale motor tests now seems explainable in terms of relative oxidation potential. Because of higher heat-transfer coefficients, and hence higher rates of diffusion of water vapor, the PSB subscale oxidation parameters are several times greater than those corresponding to the full-scale case. As a result, heat-flux rates would actually have been lower in the subscale firings because of attendantly higher surface ablation temperatures.

Within most sets of test data, motor operating conditions varied over too limited a range to observe a variation of surface temperature solely as a function of convective heat-transfer coefficient. The PSA firings, however, constitute somewhat of an exception, average chamber pressures having varied from 409 to 528 psi. For this group of data, a distinct increase in surface temperature is seen to accompany increased convective coefficients. Going from one propellant chemistry to the next, however, surface temperatures tend to decrease with increasing heat flux since the hotter

(more aluminized) exhaust environments are generally less oxidizing.

A certain degree of nonlinearity is evident in Figs. 9 and 10. A detailed discussion of the point distributions will not be attempted, however, since the precise form of these distributions has been observed to vary depending upon the methods of evaluating exhaust properties, heats of ablation, and surface regression rates. The broad qualitative aspects of the correlation persist regardless of the exact analytical techniques employed.

Analysis of Surface Composition

A semiquantitative analysis of the surface composition of postfired inserts is presented in Table 2. The object of this analysis was to detect any variation in surface composition which might be related to exhaust environmental conditions. To obtain specimens characteristic of composition exactly at the surface, replications of a few hundred microns thickness would be required. As a preliminary analysis, however, specimens were obtained by circumferentially grinding the insert surfaces to a depth of approximately 0.1 mm. Measurements were confined to samples removed from the throat regions of four subscale nozzles, which had been exposed to the propellant systems indicated in the first footnote to Table 2.

The results of the spectrographic analysis revealed an extensive deposition of propellant exhaust products. By comparing the data with propellant constituents, it could be definitely established that such deposition had taken place. The high percentages of Fe, Cu, Cr, and Mg, for example, correspond to the presence or absence of such constituents as ferrocene, copper chromite, and magnesium oxide in the individual propellant matrices. Whether such deposition occurred during equilibrium burning, during motor tailoff, and/or during residual burning at atmospheric pressure is not known.

Table 2 Insert surface composition

Element or compound	Specimen[a] 1	2	3	4
Spectrographic analysis, wt %				
Al	8–12	9–13	8–12	14–16
Si	6–9	6–9	7–10	9–11
Fe	0.5–1.0	0.2–0.6	0.4–0.9	1–2
Cr	1.0–1.5	0.6–1.1	0.06–0.11	0.06–0.11
Mg	1.5–2.5	0.15–0.26	0.15–0.25	0.75–1.25
Cu	0.01	1–2	0.01	0.01
Ti	0.2–0.5	0.2–0.5	0.2–0.5	0.2–0.5
Ca	0.15	0.15	0.15	0.6–1.0
B	0.01	0.01	0.01	0.01
Mn	0.01	...	...	0.01
X-ray diffraction results[b]				
Al	*P*	...	...	...
$\alpha - Al_2O_3$	*S*	*P*	*P*	*P*
$\iota - Al_2O_3$	...	*S*	*S*	*S*
Estimated[c] composition, wt %				
Al	10.00	...	...	...
Al_2O_3	...	20.80	18.90	28.30
$Si(O_2)$	16.10	16.10	18.25	21.50
$Fe(_2O_3)$	1.07	0.57	0.93	2.14
$Cr(_2O_3)$	1.10	1.25	0.12	0.12
Mg (O)	3.32	0.34	0.33	0.16
Cu (O)	0.01	1.88	0.01	0.01
Ti (O_2)	0.58	0.58	0.58	0.58
Ca (O)	0.21	0.21	0.21	0.21
B $(_2O_3)$	0.03	0.03	0.03	0.03
Mn (O)	0.01	...	...	...
C[d]	50.00	50.00	50.00	50.00
	82.43	91.76	89.36	104.97

[a] Specimens reflect exposure to the following propellant systems: 1) 2% Al/polysulfide; 2) 12% Al/nitrile; 3) 15% Al/composite double base; and 4) 16% Al/PBAA.
[b] *P* = primary and *S* = secondary.
[c] Based largely on spectrographic data; parentheses denote assumed oxide compounds.
[d] Based on copper electrode measurements.

One interesting result of the x-ray diffraction measurements was the discovery of free aluminum in the polysulfide-fired sample. This is a clear indication of incomplete combustion and would partially explain the correspondingly low ablation rates. In the other surface samples, x-ray diffraction detected only α and ι aluminum oxide. Except for a faint indication of β quartz, no silica was observed. Since silicon metal was identified spectrographically (Table 2), surface silica is probably present in the amorphous form. This does not preclude the possibility that silica is being reduced to free Si in the presence of carbon. Additional chemical analysis would be required, however, to distinguish between amorphous silica and free Si. Although silicon carbide is clearly visible in the upstream (high-pressure) region of the nozzle entrance cones, none was detected by x-ray diffraction at the throat location. Small percentages may actually be present, however, since crystalline compounds in amounts less than 5% of sample weight are often imperceptible by diffraction measurement. Likewise, the presence of oxides, carbides, and nitrides of the other metallic elements would also be obscured.

Special copper electrode tests were employed to establish weight fractions of uncombined carbon in the surface specimens. In each case, the concentration of carbon was reported to be approximately 50%. But in the pyrolysis of phenolic resin, only 50% of the resin by weight remains as carbonaceous residue. Barring reactions between the refrasil fiber and adjacent carbon, the char matrix for an initial composition of 75–25 refrasil-phenolic should contain no more than 14.3 wt % of carbon. Together with the low measured silica content, a 50% carbon content suggests the production of excess carbon as predicted by the equilibrium calculations. Whether this carbon is a product of resin pyrolysis, or merely a layer of soot deposited during residual burning at atmospheric pressure, has not been established.

The estimated compositions in the lower part of Table 2 assume that iron, chromium, magnesium, etc., are present in the form of high-boiling-point oxides. For specimen 1, considerably less of the total sample weight appears accounted for than in the case of specimens 2, 3, and 4. This is probably so because all of the aluminum has been treated as though it appeared only in the free metallic state, whereas x-ray diffraction indicates that a certain fraction, at least, exists as α aluminum oxide.

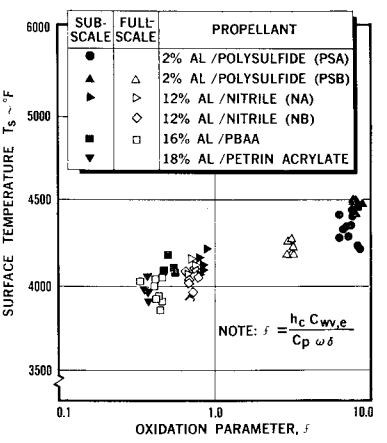

Fig. 10 Surface temperature correlation, logarithmic display.

Discussion and Conclusions

Despite the apparent correlation exhibited in Figs. 9 and 10, the details of the oxidation concept remain largely speculative. Progressive inaccuracies in heat-transfer theory, for example, might have produced the ostensible variation in ablation temperature. Change in surface emission characteristics, rather than in actual temperature level, may be the more important consequence of a varying surface composition. On the other hand, assuming that such a temperature variation occurs, other mechanisms may be responsible. It is conceivable, for instance, that as the environment becomes more oxidizing, increased energy release, and not variation in surface composition per se, causes surface temperatures to increase. This does not seem likely, however, since the predominant reaction is assumed to be the oxidation of carbon by water vapor; this is an endothermic process and would tend to lower surface temperatures.

Perhaps the most reasonable alternative to the oxidation concept is one which involves the rate of formation of SiC. In the analysis employed in this study, decomposition of the carbon-silica system is theoretically confined to temperature levels at which the equilibrium production of SiC is negligible. Thus, the concentration of carbon available to the reaction in Eq. (8) is theoretically undepleted through prior consumption in the reaction in Eq. (10). But if Eq. (10) actually proceeds to any finite extent, the availability of carbon to the reaction in Eq. (8) would be reduced accordingly. Since the extent of SiC formation would depend on the overall ablation rate, i.e., on the residence time of carbon and silica molecules in the temperature regime most favorable to its production, lower ablation rates would tend to produce glassier surface layers. Such a mechanism would be in accordance with the apparent trend of the test data. Unfortunately, the kinetic data necessary to further analyze such effects are not presently available.

In analyzing the transport of water vapor to the insert surface, a very cursory mathematical treatment has been employed. But until the importance of oxidation effects can be more firmly established, a highly refined analysis does not seem warranted. Moreover, the assumption of diffusion-controlled oxidation, although consistent with the usual treatment of graphite behavior under similar conditions, is in itself debatable. The assumption of diffusion control becomes more plausible, perhaps, if the limiting step is imagined to be the transport of water vapor within the carbon-silica melt layer. Since this entire concept involves a competition between silica and external water vapor for the available carbon atoms, the penetration of the reaction zone by water vapor might actually be viewed as a condition essential to the proposed ablation model. Such penetration could occur through turbulent transport of adsorbed water vapor within the melt layer or by diffusion of water vapor into the voids created by the escaping resin pyrolysis products. The postulation of such transport phenomena is supported both by the observed porosity of the melt layer[5] as well as from a consideration of the extent to which internal reaction proceeds in the oxidation of high-density graphite.[10]

Examination of insert surface specimens revealed extensive exhaust deposition. Since these deposits may have occurred during residual burning, little can be inferred about the nature of the surface during steady-state ablation. Measurements of this kind would be better suited to surfaces exposed to simple bipropellant systems (e.g., hydrogen-oxygen) conducted under carefully controlled conditions. To this end, a series of subscale nozzle firings are to be conducted. This program will employ a liquid and/or gaseous propellant system operating at representative pressure and temperature levels. The ablative behavior of refrasil-phenolic throat inserts will then be investigated over a much wider range of oxidizing potential than was inherent in the solid propellant test conditions reported here. Particular effort will be directed at determining the temperature and physiochemical characteristics of the ablating surface.

References

[1] Mayer, E., "Analysis of convective heat transfer in rocket nozzles," ARS J. **31**, 911–917 (1961).

[2] Arne, C. L., "The ablation of silica base materials," Douglas Aircraft Co., Inc., Santa Monica Rept. SM-44091 (July 1963).

[3] Svaton, E. M. and Winer, M., "Radiative transfer from gas-particle systems," Douglas Aircraft Co., Inc., Santa Monica Rept. SM-42607 (November 1962); also "Radiant heat transfer to the wall of a cylinder from aluminum oxide particle clouds," Douglas Aircraft Co., Inc., Paper 1768, First Annual One-Day Meeting of the Southern California Section, American Institute of Chemical Engineers, Los Angeles, Calif. (April 1964).

[4] Beecher, N. and Rosensweig, R. E., "Ablation mechanisms in plastics with inorganic reinforcement," ARS J. **31**, 532–539 (1961).

[5] Carey, M. D. and Coulbert, C. D., "Experimental chemical kinetic effects in ablative composites," Bull. Sixth Liquid Propulsion Symp. **1**, 137–152 (September 1964).

[6] Beecher, N. and Rosensweig, R. E., "Theory for the ablation of Fiberglas-reinforced phenolic resin," AIAA J. 1, 1802–1809 (1963).

[7] Kendall, R. M. and Rindal, R. A., "Analytical evaluation of rocket nozzle ablation," AIAA Preprint 64-101 (1964).

[8] Gilbert, M., Davis, D., and Altman, D., "Velocity lag of particles in linearly accelerated combustion gases," Jet Propulsion **25**, 26–30 (1955).

[9] Hidalgo, H., "A theory of ablation of glassy materials for laminar and turbulent heating," Avco-Everett Research Lab. Rept. 62 (June 1959).

[10] Ward, T. E., "Graphite erosion in a solid propellant exhaust environment," Douglas Aircraft Co., Inc., Paper 1767, First Annual One-Day Meeting of the Southern California Section, American Institute of Chemical Engineers, Los Angeles, Calif. (April 1964).

[11] Eckert, E. R. G. and Drake, R. M., Jr., *Introduction to the Transfer of Heat and Mass* (McGraw-Hill Book Co., Inc., New York, 1950), pp. 249–254.